

Static Testing of a Conductively-Cooled, High Temperature Superconducting Rotor for a 1.4 MW Electric Machine in a Thermal Vacuum Chamber

Justin J. Scheidler¹, Erik J. Stalcup², Thomas F. Tallerico¹

NASA Glenn Research Center, Cleveland, OH, 44135, USA

William Torres³

Wolf Creek Federal Services, Cleveland, OH, 44135, USA

Kirsten P. Duffy⁴

University of Toledo, Toledo, OH, 43606, USA

Tysen T. Mulder¹

NASA Glenn Research Center, Cleveland, OH, 44135, USA

NASA's high efficiency megawatt motor (HEMM) is a partially superconducting, 1.4 MW electric machine designed for electrified aircraft propulsion. HEMM's high performance is enabled by a field winding composed of 2nd generation high temperature superconducting (HTS) coils that are designed to operate at temperatures below 62 K. The superconducting rotor is conductively cooled to cryogenic temperatures using a rotating cryocooler embedded inside the machine's shaft. This paper presents a static test of the full-scale superconducting rotor in a thermal vacuum chamber. The experimental setup is described in detail. Thermal and electromagnetic 3D finite element analyses of the experimental setup are shown along with a comparison of the model results to model results for HEMM. The thermal response during cool down from room temperature is discussed. Electrical measurements are presented for operation at different dc current excitations up to the rated current of the rotor (57.2 A) and temperature limit of the HEMM design (62 K). The results suggest that minor damage to one superconducting coil occurred at 50 A and 61.2 K, causing increased resistance in the system, but that the system could still be stably operated at 57.2 A and 62 K when conductively cooled by a cryocooler.

I. Introduction

Aircraft with electrified propulsion systems will require electric machines that are very lightweight and highly efficient. Advancements to the state of the art are needed to meet this demand. This is particularly true for large transport aircraft (more than about 150 passengers), which will require electric machines with power ratings in the 1

¹ Research Aerospace Technologist, Structural Dynamics, Rotating and Drive Systems Branch, Materials and Structures Division.

² Aerospace Technologist, Heat Transfer, Thermal Systems and Transport Processes Branch, Propulsion Division.

³ Electrician, Maintenance Management Branch, Facilities Infrastructure Division.

⁴ Senior Research Associate, Mechanical, Industrial and Manufacturing Engineering Department, AIAA Member.

to 30+ MW range [1], [2]. At these power ratings, superconducting machines become an attractive option for electrified aircraft propulsion [3]. Superconducting machines can enable a mass reduction relative to non-superconducting machines directly through an increase in the machine's specific power and indirectly through a reduction in waste heat generated, which reduces the mass of the aircraft's thermal management system [4].

NASA's high efficiency megawatt motor (HEMM) is a 1.4 MW partially superconducting machine that is being developed for electrified aircraft applications. HEMM has performance goals of efficiency greater than 98% and electromagnetic specific power greater than 16 kW/kg [5] [6]. HEMM is composed of a 9 phase stator with copper windings that operate above room temperature and a cryogenic wound-field rotor with no-insulation 2nd generation high temperature superconducting (HTS) field coils. The superconducting coils are designed to be conductively cooled to less than 62 K by a pulse tube cryocooler embedded inside and rotating with the rotor shaft.

This paper presents a full-scale, static demonstration of HEMM's superconducting rotor in a thermal vacuum chamber at the designed operating temperature, current, and magnetic field. The test was developed to reduce risks associated with the thermal design of the rotor and the performance of its superconducting coils. Specifically, the objective was to measure the temperature distribution in the rotor and to demonstrate stable operation of the HTS coils under relevant thermal, magnetic, and electrical loading while being conductively cooled. Validating stable operation of the superconducting coils at less than 62 K is a key result as all prior electrical tests of HEMM's superconducting coils were conducted in liquid nitrogen (77 K) [7], [8]. No testing of the thermal design was previously completed. These test results are being used to identify design improvements to implement before an upcoming critical design review.

The paper is organized as follows. Section 2 provides an overview of HEMM and its superconducting rotor. Section 3 details the experimental setup, including the physical assembly, instrumentation, and simulated thermal and electromagnetic responses. Section 4 presents the experimental results, including the efficacy of the HEMM design and temperature gradients across critical thermal contact interfaces. Section 5 presents the conclusions.

II. Overview of HEMM and its Superconducting Rotor

HEMM is sized to satisfy the requirements of each generator of the Single-Aisle Turboelectric Aircraft with Aft Boundary Layer (STARC-ABL) concept [9]. The key performance parameters of HEMM – an efficiency >98% and an electromagnetic specific power of >16 kW/kg – can enable meaningful reductions in the fuel burn of this concept aircraft [4]. The machine is designed to produce 2 kNm of torque at a speed of 6,800 rpm. This is achieved using a rotor tip speed of only 107 m/s (Mach 0.31). The main subassemblies of HEMM are depicted in Fig. 1. The stator employs a copper armature winding that is oil cooled and operates at an average temperature around 423 K (150 °C) [10]. The field windings on the rotor are composed of 2nd generation high temperature superconducting (HTS) coils that operate below 62 K (-211 °C) [6], [7], [11]. The rotor is conductively cooled using a rotating, Stirling-type, pulse tube cryocooler that is integrated inside the machine's shaft [12], [13]. Hence, HEMM is a cryogen-free machine that appears to be the same as a non-superconducting machine from the perspective of the aircraft. The field coils on the rotor and the stator winding of the cryocooler's linear motor are both powered using a slip ring. The slip ring's rated direct current for the field winding is 75 A.

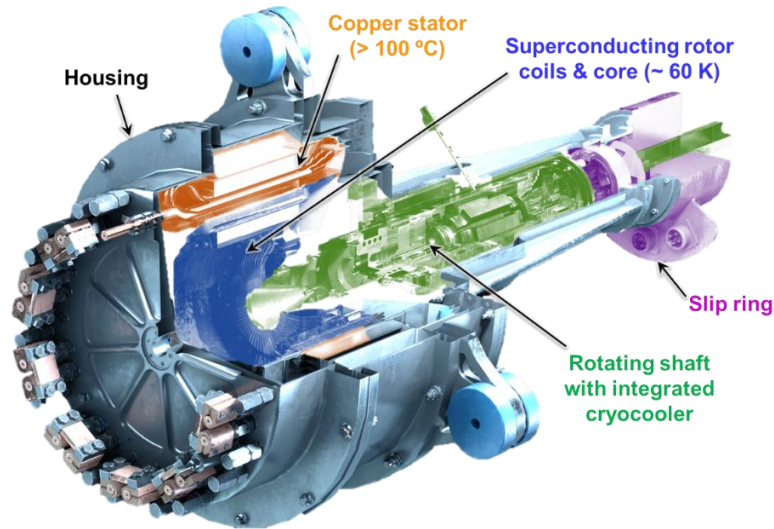


Fig. 1 Subassemblies of NASA's high efficiency megawatt motor (HEMM).

Figure Fig. 2 depicts the superconducting rotor in more detail. The rotor contains 12 poles, which results in a fundamental electrical frequency of 680 Hz. Each pole is formed by a no-insulation four-layer racetrack coil that nominally contains 600 turns of HTS (i.e., 150 turns per racetrack). The racetrack coil layers in each pole are electrically connected using HTS jumpers. The poles are electrically connected in series using redundant copper jumpers. Two copper current leads connect the rotor coils to the slip ring. The wire gauge and length of these leads were designed to minimize the heat load on the cryocooler (i.e., Ohmic loss in the leads and heat conduction along the leads from outside the cryostat). Heat conduction into the rotor is further reduced using a thin (1 mm thick) titanium shaft. Convective heating of the rotor and windage losses are significantly reduced by using HEMM's stator to form a vacuum vessel around the rotor. Pressure in the vacuum is targeted to be less than 10^{-3} torr. Radiative heating of the rotor is made small by using a low emissivity paint on the inside of the stator components that form the vacuum vessel and by gold plating most of the rotor components. The cold head of the cryocooler is connected to the rotor's back iron by a copper thermal bridge that is designed to have high thermal conductance while minimizing torsional coupling between the rotor and the cryocooler. Heat in the superconducting coil is transferred to the cryocooler through mechanical contacts to the titanium structure and back iron, through a bolted interface to the thermal bridge, and a bolted interface to the cryocooler's cold head.

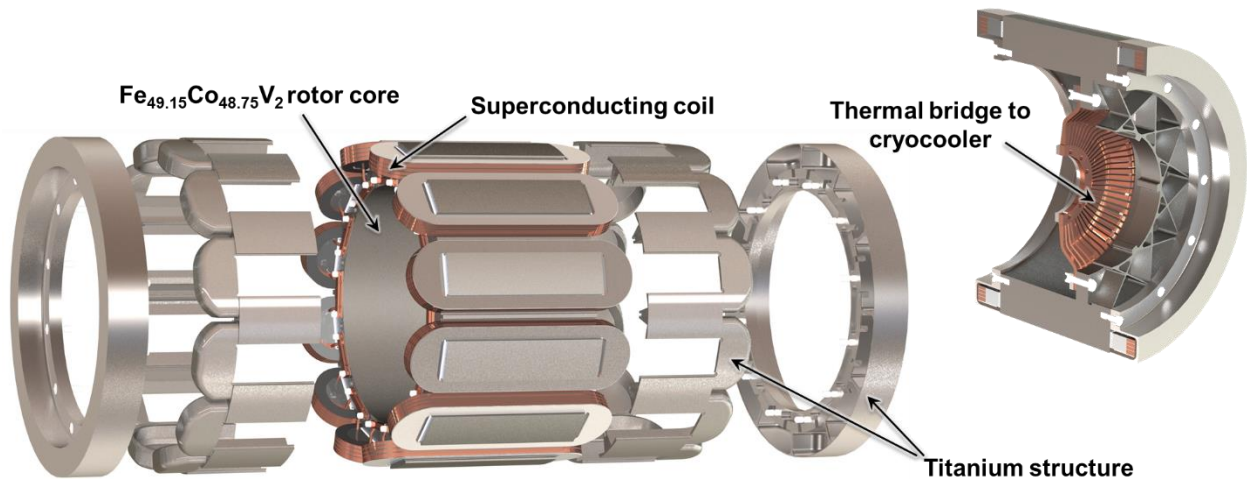


Fig. 2 Exploded and section views of HEMM's superconducting rotor.

III. Experimental Setup

This section describes the physical assembly of the experiment and its differences from HEMM. The instrumentation used in the experiment is described. A prediction of the thermal and electromagnetic performance of the experimental assembly is presented and compared to the predicted performance of the actual HEMM rotor.

A. Physical Assembly and Instrumentation

The experiment was conducted inside a thermal vacuum chamber known as the ICE-Box [14], which is located at the NASA Glenn Research Center. The ICE-Box is depicted in Fig. 3. The test rig utilizes a Gifford-McMahon cryocooler that can reach 12 K under no load and lift 100 W at 25 K. The cryocooler always operates at full capacity, so the test article's temperature was controlled using heaters installed onto the cryocooler's cold tip. A vacuum was established inside the ICE-Box's pressure vessel by continuously running a scroll pump that produced an absolute pressure of 1.6×10^{-2} torr before the cryocooler was turned on. With the cryocooler running, the pressure dropped as low as 3×10^{-5} torr due to cryopumping. Data was collected when the pressure was between 3×10^{-5} and 3.2×10^{-4} torr. In this test, the vessel's feedthroughs accommodated 15 channels for negative temperature coefficient resistive temperature detectors (RTDs), 9 channels for Type E thermocouples, 1 voltage probe, heaters for the cryocooler, heaters for the rotor's hot thermal boundary condition, and 2 high current leads (in and out).

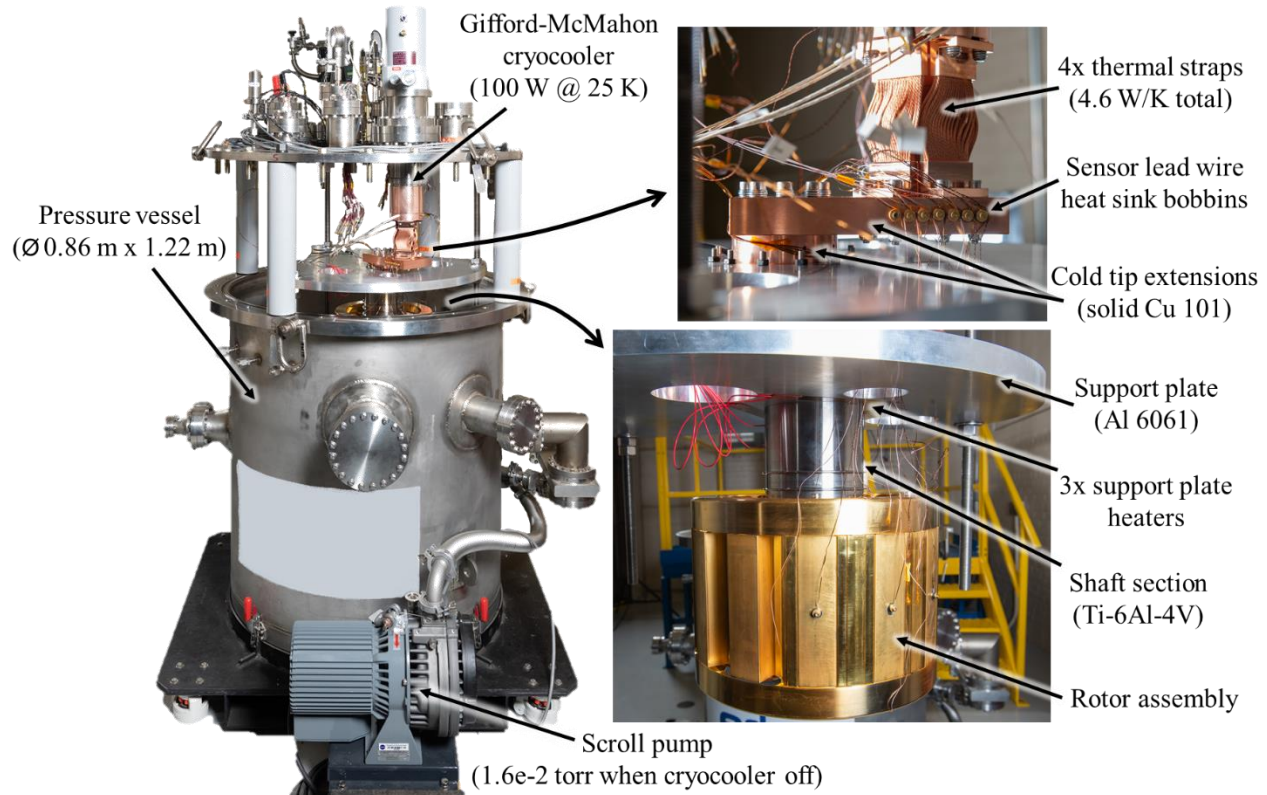


Fig. 3 ICE-Box test rig (shown with its lid raised) with test article installed and close up images of the cryocooler cold tip and rotor assemblies.

Figure Fig. 3 also shows the test article assembly. A full-scale version of HEMM's superconducting rotor was mechanically supported by a short section of the shaft from the complete machine. The rotor was secured to the shaft using a custom disk spring and snap ring assembly. The shaft was bolted to a large support plate that hangs from the lid of the ICE-Box. The plate was heated to maintain a constant temperature ranging from about 0 °C (heaters off) to 90 °C (slightly less than the predicted temperature of the shaft where HEMM's vacuum seal and cryocooler dissipate heat). The length of the shaft section matched the distance between the rotor and these heat sources in the full HEMM design. The current leads that excited the superconducting coils were heat sunk to the plate using small brackets and varnish to emulate how in the full machine the leads route inside the shaft and absorb heat from the cryocooler's hot components before reaching the cold end of the cryocooler and the rotor. The cold head of the ICE-Box's cryocooler was connected to the rotor's thermal bridge using a high thermal conductance assembly. This assembly was composed

of four copper thermal straps, a solid copper plate, and a solid copper cylinder. The conductive assembly and thermal bridge are depicted in the CAD-generated cross section of the test article assembly in Fig. 4 and the image in Fig. 5.

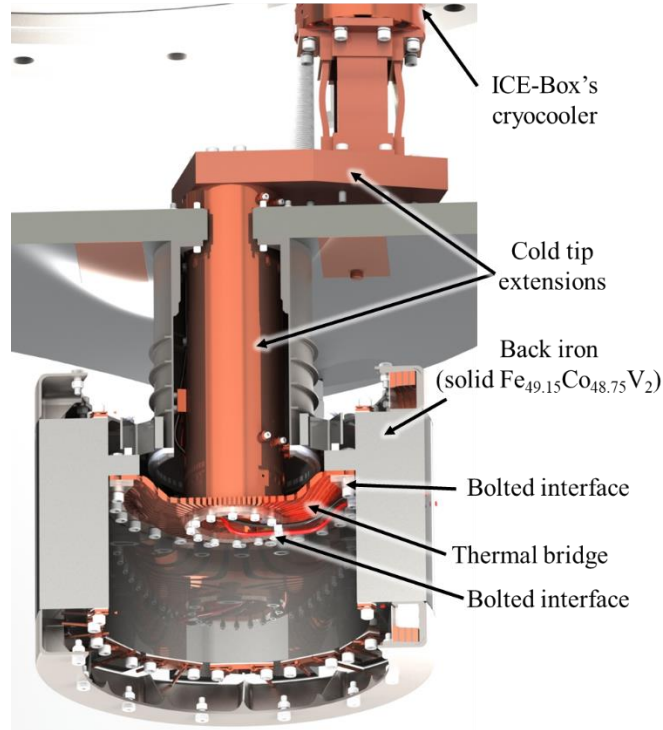


Fig. 4 CAD-generated cross section of the test article assembly.

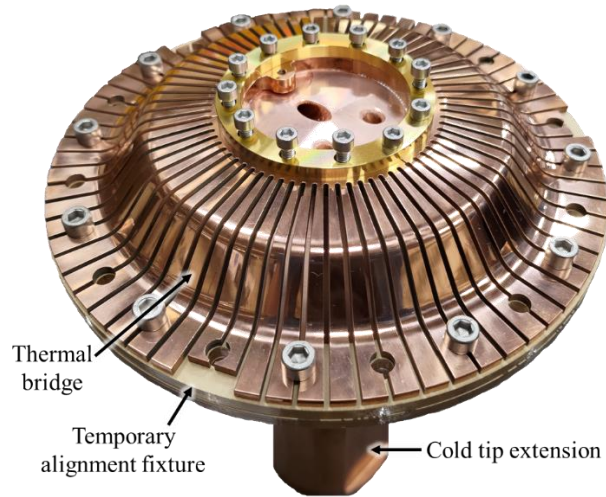


Fig. 5 Thermal bridge connected to cylindrical cold tip extension.

Thermal interface materials matching those specified in HEMM were used at all bolted joints in the assembly. The test plan specified unbolted mechanical contacts that matched the HEMM design. However, an inspection of the fabricated parts revealed that a number were at minimum material condition, causing line-to-line contact at multiple interfaces that were meant to be press fit. Consequently, a cryogenic vacuum grease was applied to these interfaces to ensure adequate thermal conductance.

To reduce the complexity and cost of the test, only three of the twelve HTS coils were included. Each HTS coil was manufactured per the HEMM design [7], [11] and installed in a titanium coil fixture. The coil assemblies were mounted on three adjacent rotor teeth and electrically connected in series with copper leads and terminals. To produce approximately the same heat as the full machine, additional copper terminals were installed around the full circumference of the back iron's axial faces and were connected by loops of copper wire that acted as surrogates for

the leads going to and from the nine missing superconducting coils. Figure Fig. 6 shows a superconducting coil in its fixture and the copper terminals and wire loops.

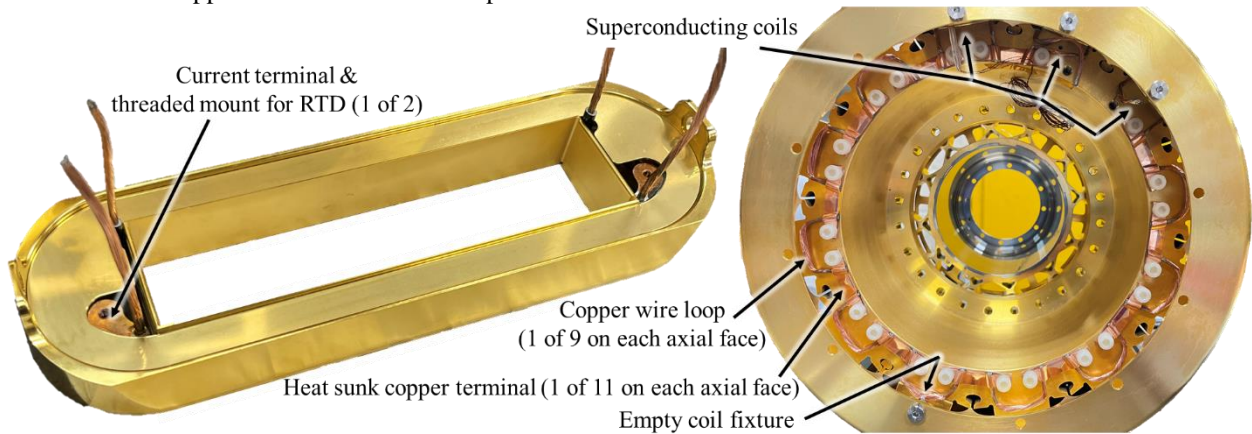


Fig. 6 One of three superconducting coils after installation into a coil fixture (left) and view of rotor's axial face showing copper current path around its circumference (right).

The location of every temperature sensor and the voltage probe is given in Fig. 7. Temperature sensors were placed to characterize the temperature of the superconducting coils, the temperature of parts in close proximity to the superconductor, and the temperature difference across mechanical interfaces. RTDs (sensors labeled CU and SD) were used at higher priority locations where higher accuracy and lower sensitivity to magnetic fields was needed. Type E thermocouples (labeled TC) were used at lower priority locations. The voltage taps (labeled V1) were connected to the terminals that the current leads are soldered to. Thus, the measured voltage includes the voltage drop across the entire current path on the rotor, including all three coils as well as all the copper coil-to-coil terminals and copper wire loops.

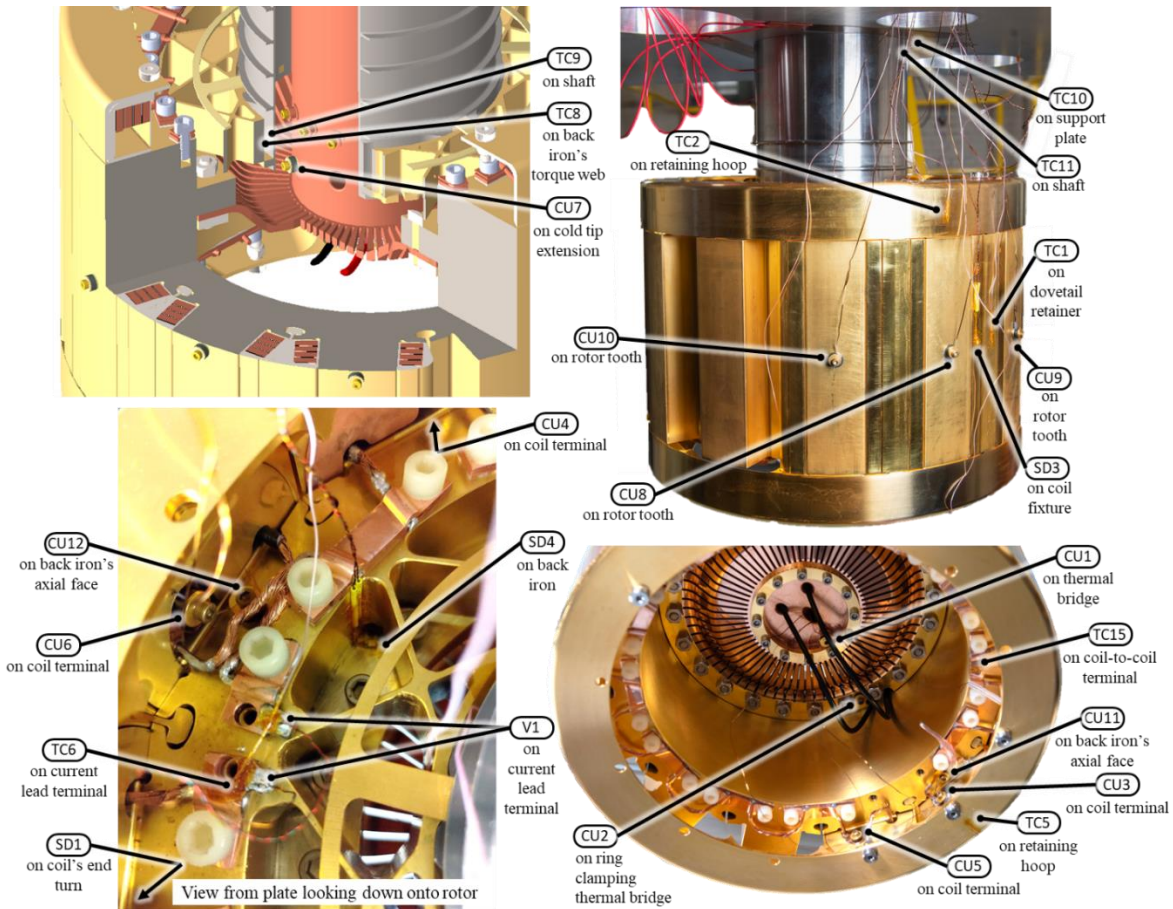


Fig. 7 Location of thermal and voltage sensors.

B. Simulated Thermal Response and Comparison to that of HEMM

3D finite element analysis was carried out on the experimental setup to quantify how well the experiment simulates the thermal environment of the actual HEMM rotor. Figure Fig. 8 shows the predicted temperature of the coils and the overall experimental assembly. Radiation, conductive, and resistive heating loads are applied in the model. Table 1 lists the magnitude of each of these heat loads in the model. The simulated cold head is assumed to be at 50 K. The coils in the experimental setup are predicted to operate at 55 K. The bulk of the rotor structure is predicted to be under 60 K. The end winding support hoops are predicted to operate at closer to 100 K in the areas where rotor coils were omitted from the experiment. The higher temperature results from the radiative heating of the end winding hoops and a highly resistive thermal path around the titanium end hoops to the coil fixtures that are included in the assembly. The end windings of the left and right coils in the experiment are predicted to have higher temperatures than the middle coils due to the heat being conducted to them by the end winding support hoops.

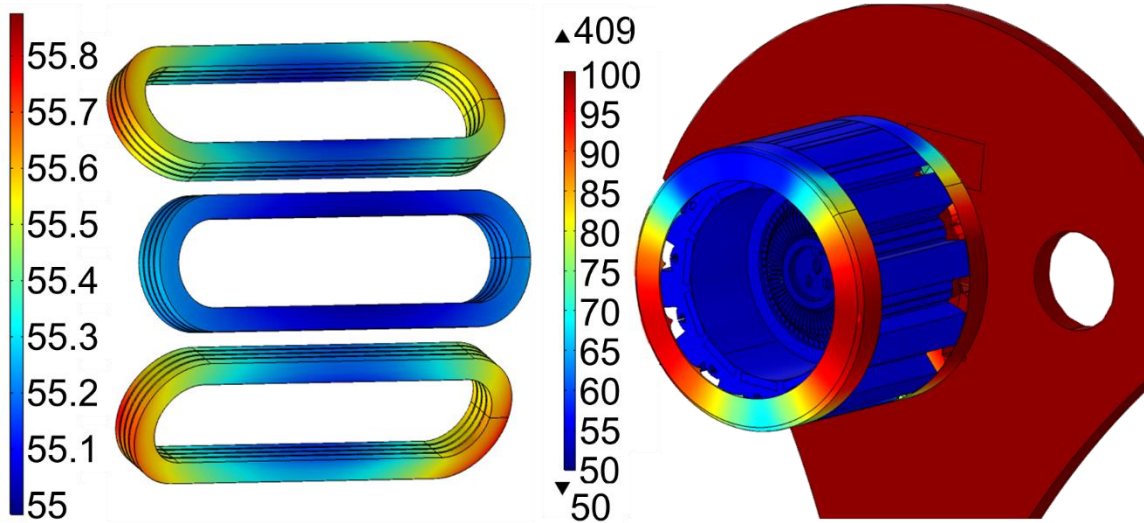


Fig. 8 Predicted temperature distribution (K) of the test article in the ICE-Box.

Table 1 Predicted rotor heat sources (W) at 50 K cryocooler cold tip.

	ICE-Box Test	HEMM
Shaft conduction	9.2	11.4
Current lead conduction	4.4	4.4
Windage & convection	0.0	5.0
Radiation	7.2	4.2
I ² R losses	3.3	3.3
Total cryocooler heat load	24.1	28.2

Figure Fig. 9 shows a comparison of the experimental setup model and a model of the full HEMM rotor. The main rotor components are shown to be around 2 K cooler in the experimental setup than they are in the HEMM rotor. Comparing coil temperatures between the two models in Table 2, the coils' maximum temperature in the experimental setup is predicted to be 1.5 K less than in HEMM. The lower temperatures in the experimental setup are primarily due to a 4 W lower heat load in the experimental setup that primarily results from windage and the associated convection that will occur in the full HEMM rotor due to rotation, which does not occur in the static ICE-Box test as indicated in Table 1.

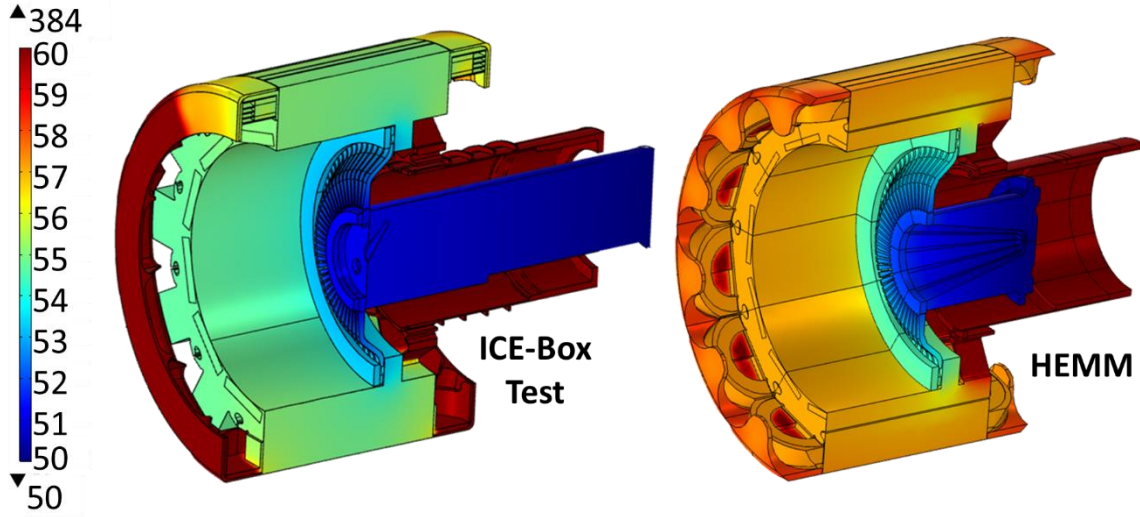


Fig. 9 Predicted temperature distribution (K) of the test article in the ICE-Box and HEMM.

Table 2 Predicted temperatures (K) of the superconducting coils.

	ICE-Box Test	HEMM
Maximum	55.9	57.4
Average	55.3	57.2

C. Simulated Electromagnetic Response and Comparison to that of HEMM

3D electromagnetic finite element analysis was conducted to design the ICE-Box experimental setup and ensure that the test setup produces a magnetic excitation on the superconducting coils that closely matches the full HEMM rotor design. The geometry used for the 3D electromagnetic model of HEMM and the separate electromagnetic model of the ICE-Box test article are shown in Fig. 10. The primary differences between the model geometries are that in the model of HEMM (a) the axial position of the back iron's torque web and flange on which the thermal bridge mounts are not up to date and (b) the stator winding and stator back iron are included. The former difference is inconsequential because prior analysis indicated that the response of the HEMM model exhibits a near negligible change when the torque web and flange are removed. The later difference is evaluated below. The rotor current (57.2 A) and number of turns per rotor coil (600) were equal in both models. Each model considered the nonlinearity of the back iron's magnetic response.

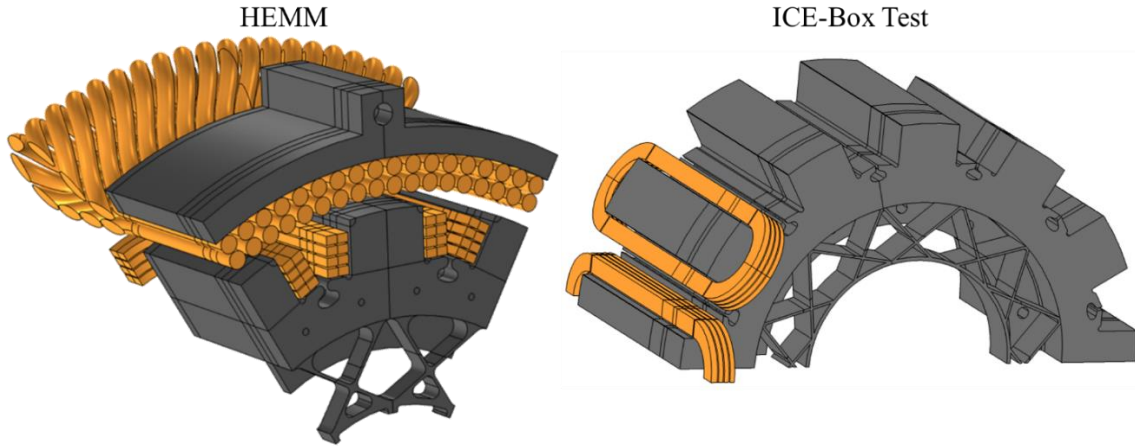


Fig. 10 Geometry used in the electromagnetic finite element model of HEMM (left) and the ICE-Box test (right).

The magnetic flux density in each layer of each superconducting coil was evaluated in both models. The predicted magnitude of the flux density at every point in the coils is depicted in Fig. 11 for both the experimental setup and the full HEMM motor. Only minor differences between the two results are observed, particularly in the end turns where critical current is often lowest. Using the magnetic flux density responses and the HEMM design method [15] (which conservatively predicts critical current), the equivalent design current for the ICE-Box test article was calculated to be 2.1 A *less* than the design current of HEMM’s rotor. The ICE-Box test article is correspondingly expected to be slightly conservative relative to the full HEMM rotor design.

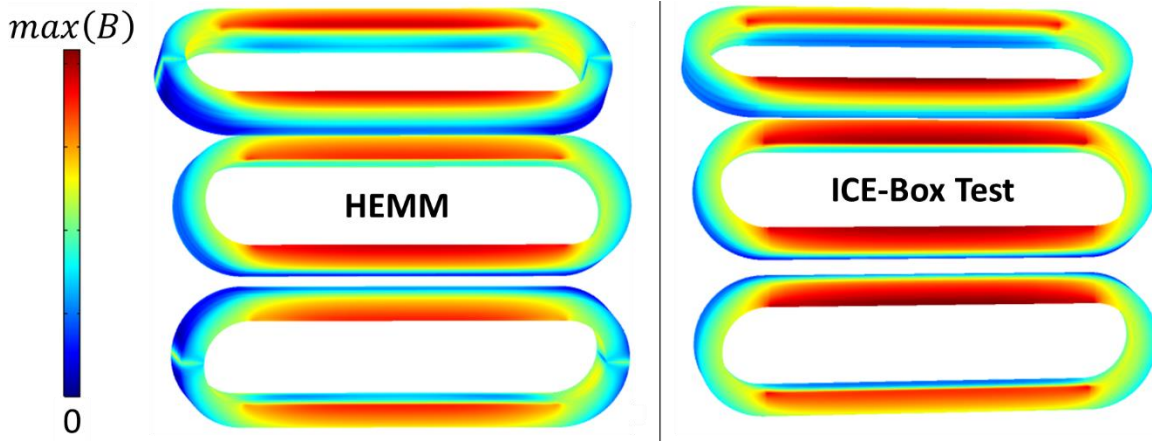


Fig. 11 Predicted magnitude of the magnetic flux density in the superconducting coils of HEMM (left) and the ICE-Box test article (right).

The omission of the stator back iron was assumed to be the likely cause of the lower predicted design current in the experimental setup. Thus, a second electromagnetic model of the ICE-Box test setup that includes the stator back iron was completed. A critical current interpolation function, described in [15], was used to predict the distribution of critical current throughout the coils of the ICE-Box test article based on the magnetic field results for the experimental setup both with and without the stator back iron. This interpolation is more precise than what has been used in the HEMM design method (and in the preceding paragraph) because it not only considers the temperature, the superconductor’s critical current at 77 K and self-field, and the magnetic flux density’s magnitude but also the flux density’s orientation. The interpolation was evaluated for each coil layer individually using the temperature prediction for each layer from Section III.C and the critical current at 77 K and self-field of the superconductor used to wind each layer of the coils for the ICE-Box test. Figure Fig. 12 shows the predicted critical current distribution in the ICE-Box test article with and without HEMM’s stator back iron. The difference in critical current is up to 68 A, but the limiting value (minimum) is nearly identical. Correspondingly, the stator back iron was not added to the experimental setup as its inclusion would have minimal impact on the maximum current that could be achieved in the ICE-Box test.

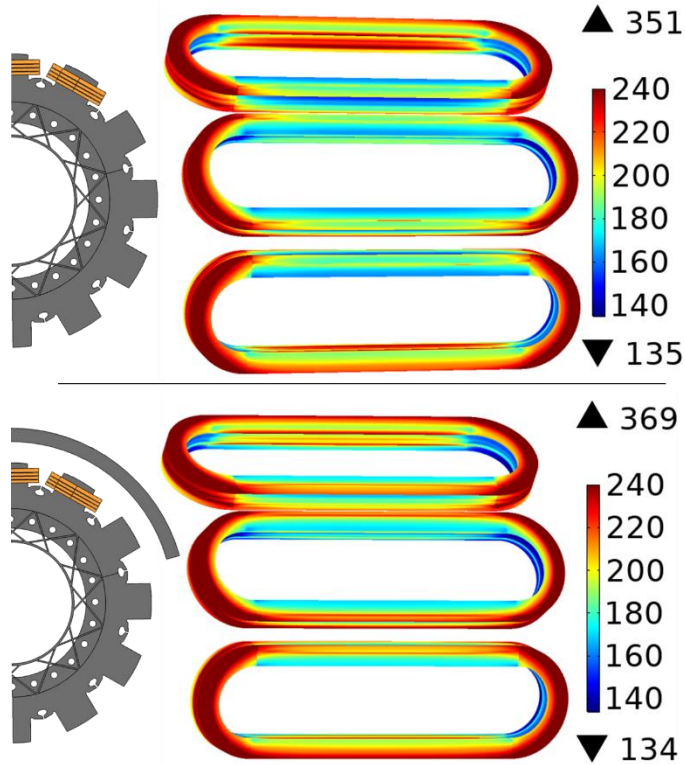


Fig. 12 Predicted critical current distribution in the superconducting coils of the ICE-Box test article with and without a stator back iron.

IV. Experimental Results – Baseline Testing in Liquid Nitrogen

Before assembling the twelve individual coil layers into the three rotor coils used in the ICE-Box test, each layer was individually tested in liquid nitrogen. The experimental setup for this baseline testing is depicted and described in [7], [8]. Coil layers were excited with direct current that was slowly ramped between setpoints from 0 to 50+ A. Voltage drop was measured across two voltage taps that were soldered onto the superconductor about 150 mm away from the current lead solder joints in an effort to measure only the response of the superconductor itself. The raw voltage measurements for each layer are shown in Fig. 13. A constant but low resistance is observed in the response of four of the coil layers. These low resistances could have resulted from the voltage taps not being far enough away from the current leads or could indicate some damage to the superconductor. Regardless, the measured resistances are relatively small and would only produce a total of 121 mW at the design current of 57.2 A. Table 3 tabulates the current in each coil layer at which the voltage began to increase nonlinearly in the liquid nitrogen test. The design current predicted by the HEMM design methodology for each layer in the liquid nitrogen test are also listed. Each coil layer is shown to have a safety factor greater than 1 when comparing these two numbers, meaning each layer can operate at the design current without the conductor going normal. Consequently, all twelve coil layers were deemed sufficiently healthy and were assembled into the three rotor coils for the ICE-Box test.

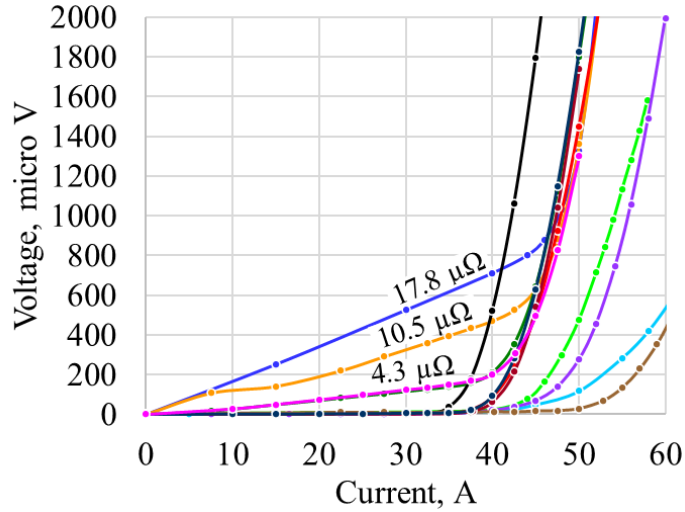


Fig. 13 Baseline electrical characterization of each racetrack coil in liquid nitrogen (77 K) with no iron core.

Table 3 Comparison of the measured safe operating current in liquid nitrogen to the value expected by the HEMM design methodology.

	Coil layer											
	1	2	3	4	5	6	7	8	9	10	11	12
Superconductor width, mm	4	3	3	3	3	3	3	4	4	3	3	3
Location in coil (1 = top, 4 = bottom)	1	2	2	4	4	3	3	1	1	4	2	3
Approximate current at start of nonlinearity, A	40	40	40	37.5	32.5	35	32.5	40	47	37.5	37.5	37.5
Designed operating current per HEMM design method, A	39	33.2	33.2	31.9	31.9	29.9	28	37.1	39	33.2	31.2	32.5
Safety factor (measured / designed)	1.03	1.21	1.21	1.18	1.02	1.17	1.16	1.08	1.22	1.13	1.20	1.15

V. Experimental Results – ICE-Box Testing

A cool down of the rotor assembly from room temperature to operating temperature was completed in about 9 hours. The duration required for HEMM may be considerably different for two reasons. First, the cold tip extensions shown in Fig. 4 add significant heat capacity to the cryogenic system, which tends to lengthen the cool down. Second, ICE-Box’s cryocooler has three to four times the heat lift as that of HEMM’s cryocooler at temperatures in proximity to 50 K, which tends to shorten the cool down. The concept of operations for HEMM has not been fully defined. If HEMM’s unassisted cool down time is unacceptable for aircraft applications, a purge of cold gaseous nitrogen could shorten the time. The current estimate for cooling down HEMM is about 10 hours, although that will be refined in future work after validating the thermal model with the data from this test.

The temperature of the ICE-Box’s cryocooler was adjusted until the measured temperatures of the superconducting coils were about 60.5 K or less. At operating temperature, span of about 2 K was observed in the temperature measurements on the superconductor and the coils’ copper terminals. The highest of the measured temperatures was sensor CU6 on the central coil’s terminal that directly connects to the current leads. The measured temperature on CU6 at the start of the first round of electrical testing was about 60.5 K. To produce the condition at the start of the first round of electrical testing, the cold tip extension had to be cooled down to a temperature of about 45.5 K at the location of sensor CU7. The measured temperature difference of about 15 K from the cold tip extension to the coil terminal instrumented with CU6 is about 9 K greater than predicted in the FEA model from Section III-C. Further testing of this test article is ongoing to investigate the cause of this higher-than-expected temperature difference. A preliminary assessment of the rotor’s thermal performance in the test suggests a few possible causes: (a) the current leads may be conducting more heat into the coils than expected, due to excess lead lengths and potentially poor thermal

contacts between the lead wires and the cold tip extension or rotor back iron and (b) the thermal conductance through the bolted interface between the thermal bridge and back iron may be underperforming. The initial electrical characterization of the rotor was carried out with this lower-than-expected thermal performance. Future work will attempt to improve the rotor's thermal performance and repeat the test with a more uniform thermal environment.

Two attempts were made to get the coils to their full operating current in this initial round of testing. The results of the first electrical characterization are depicted in the left plot of Fig. 14. Each data point was recorded at constant current after the voltage and temperature exhibited little variation; typically, about 30 minutes was required for voltage and temperature to be sufficiently stable after each current increase despite very slowly ramping the current (about 0.5 to 0.7 A/min) between setpoints to minimize AC losses inside the coil. The long duration for the coils' voltage and temperature to stabilize is primarily due to the lack of electrical insulation between the coils' turns combined with the high inductance and low resistance of the system. As current was increased in this first characterization, the highest coil temperature measurement (sensor CU6) tended to increase but was controlled to be between about 60.5 to 61.0 K by adjusting the temperature of the cryocooler. The voltage had a highly linear relationship to the applied current with a small resistance of 0.22 mΩ up to a current amplitude of 45 A. This low linear resistance combined with the very slow voltage response of the coils provides a good indication that the rotor is superconducting as designed. After ramping to a constant current of 50 A, the measured voltage behaved normally for about 8 minutes as the temperature at CU6 rose due to the added heat load. When the measured temperature at CU6 reached 61.2 K, the voltage rapidly jumped by about 7 mV and then appeared to behave normally (slowly decayed a small amount over 1 to 2 minutes). The first electrical characterization was aborted at this point, and current was ramped to zero.

The following day, a second attempt was made to ramp the coils to full operating current with more conservative control of the coil's temperature and current. The data from the second test is shown in the right plot of Fig. 14. The design current of HEMM (57.2 A) was successfully reached with 60.9 K temperature measured at CU6. The voltage again exhibited a highly linear response but with a 64% higher resistance (0.36 mΩ) than was measured on the first attempt at electrical characterization. This higher resistance suggests that the current path changed at the end of the first electrical characterization when voltage jumped 7 mV. The most probable cause of this is that critical current was locally reached near the interior of the central coil's end turn close to CU6 at 50 A in the first characterization due to temperature rise. Exceeding critical current likely caused local damage to the superconductor and a change to a higher resistance path. The results of the second characterization however demonstrate that the coil can still be stably operated at the design current despite this damage while being conductively cooled so long as the cryocooler can operate slightly colder to accommodate the added heat. After stably operating at 57.2 A and 60.9 K, the current was held fixed, and the temperature was slowly raised in increments to 62.0 K (design limit for HEMM's maximum coil temperature). Fig. 15 presents the measured voltage at each temperature. A linear response is again observed, suggesting that superconductivity was maintained up to 62.0 K. Based on a linear interpolation of cryogenic data on the resistivity of copper [16], the expected increase in resistivity – and thus resistance and voltage – during this temperature rise is 5.53% for very high purity copper, 3.88% for annealed OFHC copper, and 3.54% for OFHC copper cold drawn by 60%. The increase would be smaller for copper less pure than OFHC copper based on data collected and discussed in [17]. The measured increase in voltage during the second characterization is 1.40%, which is *less* than that expected due only to an increase in resistance of OFHC copper and reasonable for the resistance increase of less pure copper wire. This result also suggests that the coils were superconducting throughout this temperature excursion.

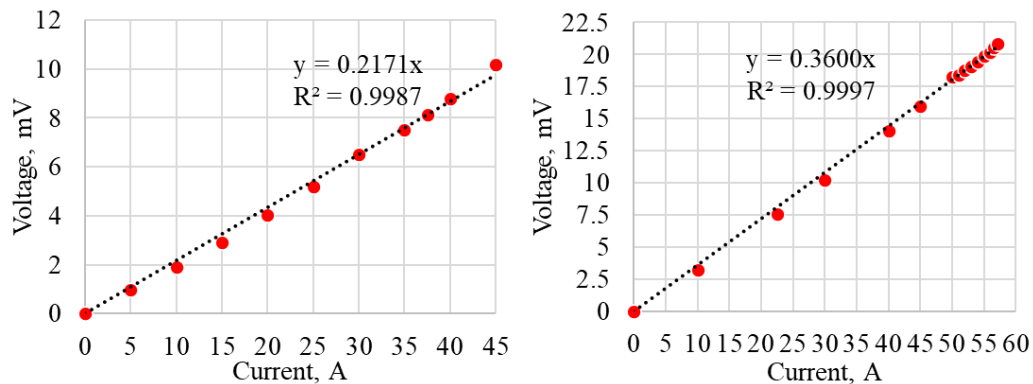


Fig. 14 Electrical characterization of the superconducting rotor before (left) and after (right) a rapid change in voltage was observed; the highest temperature of the coils was controlled within about 60.5 to 61.0 K.

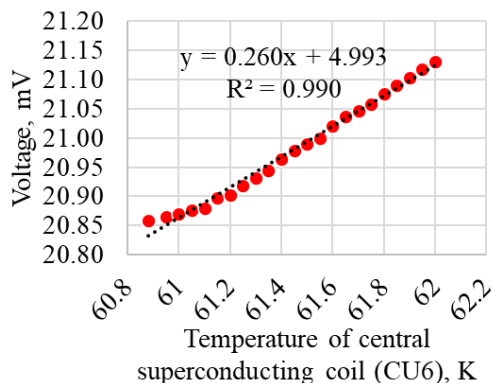


Fig. 15 Voltage across the superconducting rotor during a temperature excursion at 57.2 A.

VI. Conclusion

This paper presented the design and initial results of an experiment to demonstrate that the superconducting rotor of NASA's high efficiency megawatt motor can stably operate at the designed current and temperature. The full-scale rotor assembly that was tested included only three of HEMM's twelve high temperature superconducting coils. HEMM's stator was not included. 3D finite element analyses of the thermal and electromagnetic responses indicate that the experiment is sufficiently representative of the complete machine. The temperature over much of the rotor assembly, including the coils, is predicted to be lower in the test due in part to reduced total heat load. However, the temperature gradient in the coils is larger in the test due to the partial complement of coils. The electromagnetic behavior is slightly conservative and does not require HEMM's stator back iron to yield a reliable measurement of the rotor's superconducting response. Individual, baseline testing of all twelve coil layers in liquid nitrogen indicated that each was healthy enough to meet the HEMM design requirements. Two electrical characterizations of the rotor revealed that one coil likely experienced localized damage, but it recovered due to the no-insulation design and was subsequently able to stably operate under conductive cooling and concurrent loading up to the design current (57.2 A) and temperature limit (62 K).

Acknowledgments

This work was supported by the NASA Advanced Air Transportation Technologies Project - Propulsion & Power Subproject managed by Amy Jankovsky within NASA's Aeronautics Research Mission Directorate. The authors thank their colleague Fred Vankeuls for assisting with test rig operation and sensor troubleshooting.

References

- [1] R. H. Jansen, C. Bowman and A. Jankovsky, "Sizing Power Components of an Electrically Driven Tail Cone Thruster and a Range Extender," in *16th AIAA Aviation Technology, Integration, and Operations Conference*, Washington, D.C., 2016.
- [2] R. H. Jansen, C. Bowman, A. Jankovsky, R. Dyson and J. Felder, "Overview of NASA Electrified Aircraft Propulsion (EAP) Research for Large Subsonic Transports," in *53rd AIAA/SAE/ASEE Joint Propulsion Conference*, Atlanta, GA, 2017.
- [3] G. V. Brown, "Weights and Efficiencies of Electric Components of a Turboelectric Aircraft Propulsion System," in *49th AIAA Aerospace Sciences Meeting*, Orlando, FL, 2011.
- [4] S. L. Schnulo, J. W. Chapman, P. Hanlon, H. Hasseeb, R. H. Jansen, D. Sadey, E. Sozer, J. Jensen, D. Maldonado, K. Bhamidipati, N. Heersema, K. Antcliff, Z. J. Frederick and J. Kirk, "Assessment of the Impact of an Advanced Power System on a Turboelectric Single-Aisle Concept Aircraft," in *AIAA/IEEE Electric Aircraft Technologies Symposium (EATS)*, virtual, 2020.
- [5] R. H. Jansen, Y. De Jesus-Arce, P. Kascak, R. Dyson, A. Woodworth, J. J. Sheidler, R. Edwards, E. Stalcup, J. Whillite, K. Duffy, P. Passe and S. McCormick, "High Efficiency Megawatt Motor Conceptual Design," in *AIAA Propulsion and Energy Forum*, Cincinnati, 2018.

- [6] R. H. Jansen, P. Kascak, R. Dyson, A. Woodworth, J. Scheidler, A. D. Smith, E. Stalcup, T. Talerico, Y. De Jesus-Arce, D. Avanesian, K. Duffy, P. Passe and G. Szpak, "High Efficiency Megawatt Motor Preliminary Design," in *AIAA/IEEE Electric Aircraft Technologies Symposium (EATS)*, Indianapolis, IN, 2019.
- [7] J. J. Scheidler, T. F. Talerico, W. A. Miller and W. Torres, "Progress Toward the Critical Design of the Superconducting Rotor for NASA's 1.4 MW High-Efficiency Electric Machine," in *AIAA/IEEE Electric Aircraft Technologies Symposium (EATS)*, Indianapolis, IN, 2019.
- [8] J. J. Scheidler, T. F. Talerico, W. Torres and W. A. Miller, "Risk Reduction Testing of Superconducting Coils for the High Efficiency Megawatt Motor," in *AIAA SciTech Forum*, San Diego, CA, 2022.
- [9] J. R. Welstead and J. L. Felder, "Conceptual Design of a Single-Aisle Turboelectric Commercial Transport with Fuselage Boundary Layer Ingestion," in *54th AIAA Aerospace Sciences Meeting*, San Diego, California, 2016.
- [10] G. Szpak, A. Smith, J. Thompson, A. Woodworth and R. Jansen, "High Efficiency Megawatt Motor Thermal Stator Preliminary Design," in *AIAA/IEEE Electric Aircraft Technologies Symposium (EATS)*, virtual, 2020.
- [11] T. T. Talerico, J. J. Scheidler, D. Lee and K. Haran, "Electromagnetic Redesign of NASA's High Efficiency Megawatt Motor," in *2020 AIAA/IEEE Electric Aircraft Technologies Symposium (EATS)*, virtual, 2020.
- [12] R. W. Dyson, R. H. Jansen, K. P. Duffy and P. J. Passe, "High Efficiency Megawatt Machine Rotating Cryocooler Conceptual Design," in *AIAA/IEEE Electric Aircraft Technologies Symposium (EATS)*, Indianapolis, IN, 2019.
- [13] K. P. Duffy, P. J. Passe, R. W. Dyson, R. H. Jansen, Y. De Jesus-Arce and A. D. Anderson, "Design, Analysis, and Testing of the HEMM Cryocooler Linear Motor," in *AIAA/IEEE Electric Aircraft Technologies Symposium (EATS)*, virtual, 2020.
- [14] J. W. Hartwig, G. Brown, B. Choi, F. Vankeuls, C. Llanes and C. Hall, "DC Performance Testing of MgB2 Superconducting Straight Wire Samples," in *AIAA AVIATION 2022 Forum*, Chicago, IL, 2022.
- [15] J. J. Scheidler and T. F. Talerico, "Methodology for Electromagnetic Optimization of a Partially Superconducting 1.4 MW Electric Machine for Electrified Aircraft Propulsion," *IEEE Transactions on Applied Superconductivity*, vol. 33, no. 5, 2023.